Cu-capped surface alloys of Pt/Cu{100}



2003 J. Phys.: Condens. Matter 15 1879

(http://iopscience.iop.org/0953-8984/15/12/305)

INSTITUTE OF PHYSICS PUBLISHING JOURNAL OF PHYSICS: CONDENSED MATTER

J. Phys.: Condens. Matter **15** (2003) 1879–1887 PII: S0953-8984(03)56596-1

# Cu-capped surface alloys of Pt/Cu{100}

**Ehab AlShamaileh[1,2], Colin J Barnes[2,4] and Adrian Wander[3]**

[1] School of Physical Sciences, Dublin City University, Dublin 9, Republic of Ireland
[2] School of Chemical Sciences, Dublin City University, Dublin 9, Republic of Ireland
[3] CLRC, Daresbury Laboratory, Daresbury, Warrington WA4 4AD, UK

Received 25 November 2002
Published 17 March 2003
Online at stacks.iop.org/JPhysCM/15/1879

**Abstract**

The room-temperature deposition of 0.5 monolayer (ML) Pt on Cu{100} followed by annealing to 525 K results in a sharp c(2 × 2) low-energy electron diffraction (LEED) pattern. The structure of this surface alloy is investigated by means of symmetrized automated tensor low-energy electron diffraction (SATLEED) analysis and *ab initio* plane wave density functional calculations. The results are then compared with those for the similar system 0.5 ML Pd/Cu{100}. SATLEED results for the Pt/Cu{100} show that it consists of an ordered c(2 × 2) Cu–Pt second layer alloy capped with a pure Cu first layer. The first and second interlayer spacings are found to be expanded by $+5.1 \pm 1.7$ and $+3.5 \pm 1.7\%$ respectively (relative to the bulk Cu interlayer spacing of 1.807 Å) due to the insertion of the 8% larger Pt atoms into the second layer. The ordered mixed layer is found to be rippled by $0.08 \pm 0.06$ Å with Pt atoms rippled outwards towards the solid–vacuum interface. A smaller rippling of $0.03 \pm 0.11$ Å in the fourth pure Cu layer was also detected with Cu atoms directly underneath Pt atoms rippled towards the second layer Pt resulting in a Pt–Cu bond length of 2.52 Å which compares with the sum of metallic radii of 2.67 Å. A recent quantitative SATLEED analysis for 0.5 ML Pd/Cu{100} was performed in an earlier study (Barnes *et al* 2001 *Surf. Sci.* **492** 55). A similar structure to the Pt/Cu{100} has been retrieved with slight differences in the interlayer spacings. The *ab initio* density functional results are fully consistent with the experimentally determined structures. However, they reveal an interesting difference between the stability of the Pd and Pt systems and highlight the fact that the Pd/Cu structure is best thought of as a metastable structure occurring as an intermediate step in the diffusion of the transitional metal ion into the bulk of the Cu substrate.

## 1. Introduction

The incorporation of catalytically active metals into the top few surface layers of another metal is an area of growing physical and chemical interest [1–5]. Cu–Pt and Cu–Pd combinations

[4] Deceased.

  

are of particular importance due to the many applications of Pt, Pd and Cu in heterogeneous catalysis including oxidation of CO and NO gases over Pt/Pd [6–8] and methanol and ammonia production [9, 10].

In contrast to the Cu{100}/Pd bimetallic combination, little work has appeared to date on the Cu{100}/Pt system. Using $He^+$ and low-energy ion scattering spectroscopy (LEISS), Graham *et al* [11] have reported that the room-temperature deposition of 0.5 monolayer (ML) Pt film on Cu{100} followed by annealing to 525 K produces an essentially Cu-terminated surface. On the contrary, Shen *et al* [12] suggested that at this coverage, annealing to 453 K for 10 min results in a surface alloy with 38 at.% Pt in the outermost layer and 10 at.% Pt in the second layer. The different top layer compositions may be attributed to the differing thermal activation procedures employed.

Recently, Reilly *et al* [13] have studied the formation kinetics of the Cu{100}–c$(2\times2)$–Pt by deposition of Pt at room temperature and monitoring the intensity and full-width-at-half-maximum of the (1, 0) and (1/2, 1/2) low-energy electron diffraction (LEED) beams as a function of temperature and time. It was concluded that annealing to 550 K for 30 s produced the maximum (1/2, 1/2) beam intensity indicating a state of optimal ordering of the c$(2\times2)$ phase. Using CO titration to probe the surface Pt concentration, Reilly *et al* reported a considerable reduction in saturation CO uptake after annealing the room-temperature deposited Pt to 550 K. This was interpreted as being due to the formation of a Cu{100}–c$(2\times2)$–Pt underlayer alloy with an outermost layer of almost pure copper due to the much higher sticking coefficient of CO on Pt compared with Cu. Using the same sticking coefficient difference argument, the authors excluded the possibility of top layer surface alloy formation based on studies of CO adsorption on $Cu_3Pt$ bulk alloys [13].

In this paper, the structure of the Cu{100}–c$(2\times2)$ 0.5 ML Pt phase is determined by symmetrized automated tensor low-energy electron diffraction (SATLEED) and by *ab initio* plane wave density functional theory. Both a surface alloy model, where the mixed layer is located in the outermost layer, and an underlayer alloy model, with the mixed layer sandwiched in the second layer, along with overlayer models with Pt occupying four-fold hollow, bridge and atop sites, are considered.

## 2. Experimental details

Details of the LEED ultra-high vacuum study have already been published [14]. In this study, the base pressure was $2\times10^{-10}$ Torr. Platinum was evaporated via resistive heating of a well-outgassed 0.25 mm diameter W wire (99.99%, Goodfellow Metals, UK) around which was wrapped high-purity 0.125 mm diameter Pt wire (99.999%, Goodfellow Metals, UK). The evaporation rate was calibrated by measuring the (1/2, 1/2) beam intensity and full-width at half-maximum. This method of calibration was used, rather than conventional Auger electron spectroscopy (AES), because it does not underestimate the true Pt coverage if deviations from layer-wise growth occur. The intensity of the (1/2, 1/2) beam was measured as a function of Pt evaporation time at a fixed incident electron energy. The deposition time needed to maximize the (1/2, 1/2) beam intensity was assigned to a Pt coverage of 0.60 ML according to a recent study by Reilly [15]. From the calibration curve constructed for the measured (1/2, 1/2) beam intensity versus deposition time, we estimate the Pt coverage to be $0.50\pm0.10$ ML.

Deposition of 0.5 ML Pt at room temperature results in a weak and diffuse high background c$(2\times2)$ LEED pattern. Annealing this phase to 525 K for 30 s produced a good-quality c$(2\times2)$ LEED pattern.

LEED $I(V)$ data were collected at close to room temperature using a CCD camera interfaced with a minicomputer for data acquisition. All spectra used in this study were

collected at normal incidence. One set of data measured for the same phase on the same day was used in the calculations.

Five non-symmetric beams (three integral, namely (1, 0), (1, 1) and (2, 0), and two fractional, namely (1/2, 1/2) and (3/2, 1/2)) were used in the analysis corresponding to a total energy range of 1300 eV. Beams were individually background subtracted and symmetry-equivalent beams were averaged to minimize errors ensuing from small deviations from normal incidence or residual magnetic fields. The beams were then normalized to constant incoming beam current and finally smoothed by a five-point adjacent-averaging prior to analysis.

Theoretical LEED $I(V)$ spectra were calculated using the SATLEED package [16]. Nine phaseshifts for both Pt and Cu were used in the calculations and were generated by the phaseshifts package of Barbieri and van Hove [17]. Initially, bulk Debye temperatures of Cu and Pt of 343 and 240 K respectively were used in the analysis [18]. A fixed value of $-5.0$ eV for the energy independent imaginary part of the inner potential was used in the initial phase of the analysis while the energy-independent real part was allowed to be optimized in the course of the calculations. The Pendry $R$-factor ($R_p$) and the $RR$-function were used to test the agreement of theory and experiment and to calculate the error bars respectively [19].

## 3. *Ab initio* plane wave density functional theory

The *ab initio* calculations were performed employing plane wave density functional theory (DFT) as implemented in the CASTEP code [20, 21]. Core electron states were represented by the use of ultrasoft pseudopotentials [22], and the calculations were found to be converged to better than 0.01 eV/atom for a plane wave cut-off energy of 400 eV. The electronic ground state was found through conjugate-gradient minimization of the total energy with respect to the plane wave coefficients. Mechanical equilibrium was achieved by relaxation of the ionic positions using a modified Broyden–Fletcher–Goldfarb–Shanno (BFGS) minimization algorithm to minimize the total energy of the system. Electron exchange and correlation were described within the generalized gradient approximation [23]. Brillouin zone sampling was performed on a Monkhorst–Pack grid with the density of points determined from a spacing of 0.05 Å$^{-1}$.

Test results of the pseudopotentials and plane wave cut-off value gave a bulk copper lattice parameter of 3.603 Å, which is in line with the experimental value of 3.604 Å [24]. Tests of convergence with respect to slab thickness and vacuum gap size were performed via the optimization of the clean Cu{100} surface geometry. The surface energy was found to be converged to better than 0.01 eV/slab unit cell for a 20 Å vacuum gap and a slab thickness of nine repeat layers. These values were utilized for all subsequent calculations. The optimum geometry was found to be a contraction of $d_{12}$ by 3.8%, an expansion of $d_{23}$ by 0.72% and a contraction of $d_{34}$ by 0.28%, in excellent agreement with the known experimental structure [25]. Hence we can have confidence that the choice of parameters and system size is sufficient to model the chosen systems.

## 4. Results and discussion

Figure 1 illustrates possible models for the Cu{100}-c(2 × 2) 0.5 ML Pt phase. Extensive LEED calculations were carried out for each model involving optimization of structural and non-structural parameters seeking the lowest $R_p$ factor. In the early stages of the analysis only the first two interlayer spacings were allowed to vary ($d_{12}$ and $d_{23}$ are measured from first-layer Cu atoms to second-layer Cu atoms in the alloy models). The ranges of variation for each

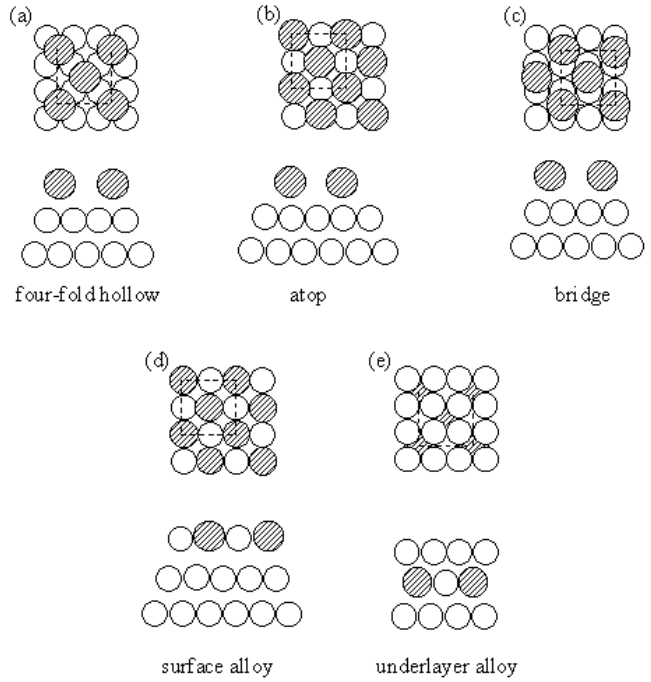


**Figure 1.** Possible models for the Cu{100}–c(2 × 2)–Pt phase including: (a) four-fold hollow overlayer; (b) atop overlayer; (c) bridge overlayer; (d) surface alloy and (e) underlayer alloy.

**Table 1.** Optimal Pendry $R$-factors for models shown in figure 1.

| Model | $d_{12}$ and $d_{23}$ ranges tested (Å) | $R_p$ |
|---|---|---|
| Four-fold hollow overlayer | 1.65–2.25 | 0.56 |
| Atop overlayer | 2.50–2.90 | 0.62 |
| Bridge overlayer | 2.00–2.55 | 0.52 |
| Surface alloy | 1.65–2.25 | 0.40 |
| Underlayer alloy | 1.65–2.25 | 0.32 |

model are indicated in table 1, which also shows the lowest total $R_p$ for the tested models. In the alloy models where mixing of Pt and Cu takes place, a buckling of about 0.3 Å was allowed for Pt atoms buckled in either vertical direction.

The results clearly indicate that the underlayer CuPt alloy yields the best agreement between theory and experiment and all other structures fell outside the $RR$-value of 17.5%. Hence, the underlayer model was considered for further optimization excluding all other models. This refinement process involved the optimization of all symmetry-allowed structural and non-structural parameters (Debye temperatures of the Cu and Pt and the energy-independent imaginary part of the inner potential) yielding an optimal Pendry $R$-factor of 0.27.

Figure 2 shows a side view of the model detailing the favoured geometric parameters. Notice that rippling in layers 1 and 3 is not allowed by symmetry. Figure 3 illustrates the comparison of experimental and calculated (best-fit) LEED $I(V)$ spectra for the favoured underlayer structure. The dependence of Pendry's $R$-factor on the first and second interlayer spacings and the rippling in the mixed CuPt layer and the fourth Cu layer are shown in figure 4.

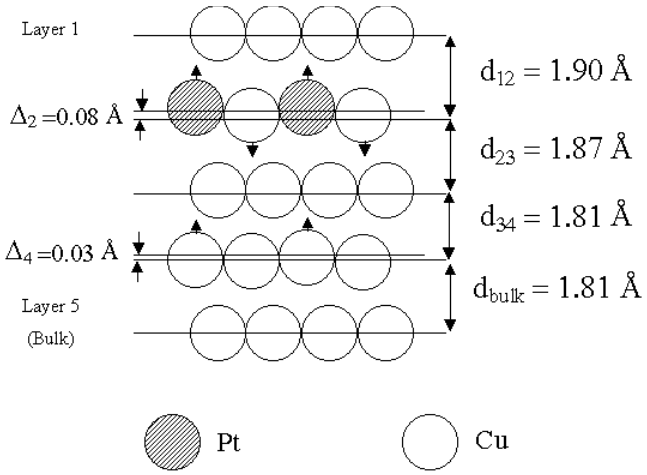


**Figure 2.** Side view along [011] direction of the favoured model showing the best-fit geometrical parameters.

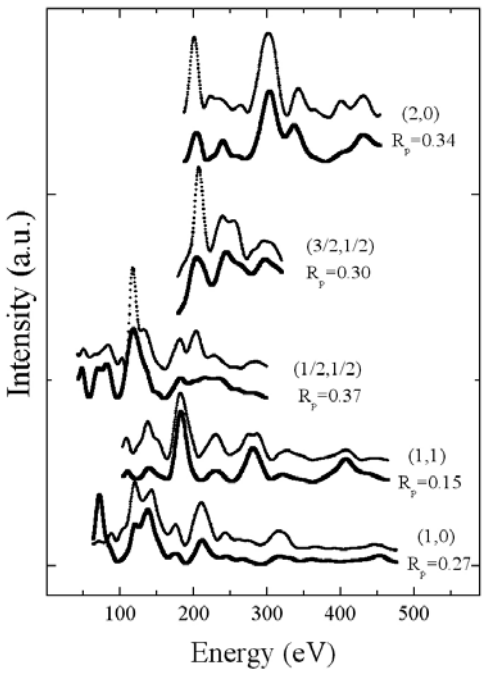


**Figure 3.** Comparison of experimental (lower solid curves) and calculated (upper dotted curves) LEED $I(V)$ spectra for each beam for the favoured Cu{100}–c(2 × 2)–Pt underlayer structure.

The favoured model consists of a mixed CuPt underlayer capped with a pure Cu layer. The first and second interlayer spacings were found to be $d_{12} = 1.90 \pm 0.03$ Å and $d_{23} = 1.87 \pm 0.03$ Å respectively, corresponding to an expansion of $5.1 \pm 1.7$ and $3.5 \pm 1.7\%$ respectively (relative to the bulk Cu value of 1.807 Å). The third interlayer spacing experienced a small expansion of $0.3 \pm 1.7\%$. A small buckling of $0.08 \pm 0.05$ Å was detected in the mixed underlayer with Pt atoms rippled outwards towards the solid–vacuum interface.

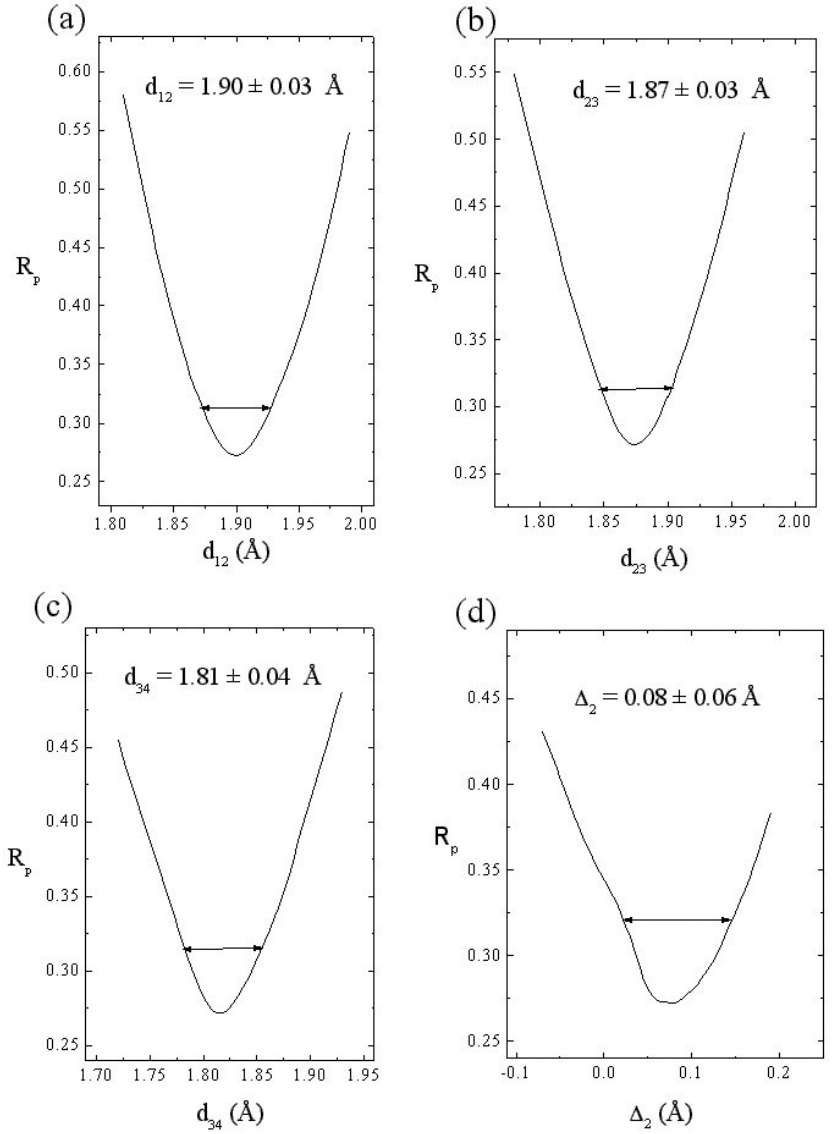


**Figure 4.** The dependence of Pendry $R$-factor on (a) the first interlayer spacing ($d_{12}$); (b) the second interlayer spacings ($d_{23}$); (c) third interlayer spacings ($d_{34}$) and (d) the buckling in the mixed CuPt layer ($\Delta_2$). The optimal value for each variable is shown at the top of each panel along with the associated error. Horizontal lines indicate the variance.

The *ab initio* density functional theory results are in line with the experimentally determined structure. A detailed comparison is presented in table 2. Both the theoretical results and the LEED results indicate a significant expansion of both the first to second and second to third interlayer spacings with all deeper layer spacings remaining at essentially their bulk value. However, it is clear that the first and second layer expansions exhibit some deviation, in that in the LEED result the first layer expansion is larger, while in the DFT the second layer expansion is larger. This difference lies within the experimental error bars. The difference in

**Table 2.** Comparison of DFT and LEED results for the Pt/Cu{100} system.

| Parameter | DFT value (Å) | LEED value (Å) |
|---|---|---|
| $d_{12}$ | 1.87 | 1.90 |
| $d_{23}$ | 1.93 | 1.87 |
| $d_{34}$ | 1.80 | 1.81 |
| Pt above Cu ($\Delta_2$) | 0.02 | 0.08 |

$\Delta_2$ obtained from the two methods (0.02 and 0.08 Å) lies within the calculation error bars. In addition, the *ab intio* calculations were also performed for a hypothetical overlayer alloy model. For this system, the results indicate a significant expansion of the first to second interlayer spacing with all other spacings being close to their bulk value. The underlayer alloy was found to be 0.28 eV/unit cell more stable than the overlayer alloy which equates to 0.14 eV/surface Pt atom since double-sided slabs have been used throughout. Again, this is in line with the experimental observation that room-temperature adsorption does not give rise to a sharp c($2 \times 2$) LEED pattern. The lower stability of the Pt adlayer does not explain the fact that there is no sharp LEED pattern for this metastable structure. The key parameters are the lateral interaction between the Pt atoms and the energy barrier between the adlayer and the subsurface layer structure.

It is interesting to compare the structure obtained in this analysis with the corresponding Cu{100}–c($2 \times 2$)–Pd underlayer alloy analysed recently by LEED $I(V)$ calculations [14]. It was found that Pd forms a mixed CuPd underlayer when a top layer surface alloy formed by deposition of 0.5 ML Pd is thermally treated [14]. Three major differences from our results can be noticed: firstly, there does not appear to be a stable CuPt overlayer ordered alloy. Secondly, in the mixed underlayer, Pd atoms are rippled inward while Pt atoms in the mixed underlayer are rippled outward towards the solid–vacuum interface. Thirdly: in the Pd system, a greater buckling was detected in the fourth Cu layer ($0.2 \pm 0.1$ Å) while in the Pt system a much smaller value is favoured ($0.03 \pm 0.11$ Å).

The CuPd system has also been investigated using *ab initio* density functional theory for comparison with the CuPt results. The geometric structure of both the overlayer and underlayer alloy systems is found to be in good agreement with the experimental data [14]. The first to second interlayer distance is found to be expanded by 0.02 Å for the overlayer system with a buckling in the first layer of 0.09 Å. For the underlayer system the first to second and second to third interlayer spacings are significantly expanded relative to their bulk values. However, within the *ab initio* calculations we do not find a substantial buckling in the fourth layer for the Pd system. Interestingly, for the Pd system we find that the energetics of the overlayer and underlayer stabilities is reversed with the overlayer alloy being more stable than the underlayer by 0.035 eV/Pd atom. This is a rather small value that is close to the lower limit of significance within the current calculational scheme. However, it does strongly suggest that the CuPd underlayer alloy is not a stable structure but is, at best, a metastable phase occurring during the bulk diffusion of the adsorbed Pd atoms. This is supported by average $T$-matrix approximation modelling of the CuPd system which suggests that a significant fraction of the adsorbed Pd is not present in the underlayer alloy. Given the uncertainties in assigning an exact composition to the individual layers within the LEED determination it may be that the discrepancy in the size of the fourth layer buckling between the theoretical and experimental results is an artefact of the LEED computational scheme.

On the other hand, the two systems depicted a similar general structure where the first and second interlayer spacings are expanded relative to the Cu bulk values. The net expansion of the

outermost three-layer slab is found to be 0.18 and 0.15 Å for the Cu{100}/Pd and Cu{100}/Pt underlayer alloys respectively. This similarity may be attributed to the almost identical sizes of Pd (12-coordinate metallic radius = 1.38 Å) and Pt (12-coordinate metallic radius = 1.39 Å) and may also be extended to the similarity of their electronic/bonding properties since they belong to the same group in the periodic table. However, caution should be applied when utilizing atomic radii to analyse the geometry of surface structures. For example, the hard sphere radii of Pd and Pt would give rise to a much greater buckling of the mixed layers within the alloy systems than is observed either theoretically or experimentally. Of course, the system is not composed of a superposition of atoms and consequently the division of interatomic distances into the sum of atomic radii cannot be performed uniquely.

When Pt atoms replace every second Cu atom in the second layer, the Cu–Pt bond length calculated between first-layer Cu atoms and second-layer Pt atoms is found to be 2.56 Å. This value corresponds to a 4.1% contraction of the sum of the 12-coordinate metallic radii of Cu and Pt of 2.67 Å. It is interesting to note that the sum of the first and second interlayer spacings in the Cu{100}–c(2 × 2)–Pt underlayer is 8.6% which is very similar to the size mismatch between Cu and Pt atoms of 8.1%. The apparent contraction of Pt atoms is a result of coordination with Cu atoms while the expansion in the first and second interlayer spacings comes from the incorporating of the larger Pt atoms into the second layer of the selvedge.

The structure retrieved in this study is in accordance with that suggested by Reilly *et al* [13] based on CO titration results. Those authors also suggested that the top layer may contain some Pt atoms (about 10% of the deposited Pt) [13]. In our study, we have modelled a relatively perfect distribution of Pt atoms in the system represented by considering a pure top Cu layer, a 50:50 mixed CuPt underlayer and pure Cu layers underneath. It is possible that the experiment–theory agreement can be improved if the average $T$-matrix approximation (ATA) technique is used to model imperfections such as low Pt concentration in layers 1 and 3 [26]. This should lead to an enhanced level of agreement between theory and experiment and a detailed picture of the layer-wise compositional profile along with small changes in surface geometric parameters to those obtained here based on assumption of a somewhat idealized layer-wise compositional profile.

Finally, it is worth noting that the {100} surface of a $Cu_3Pt$ bulk alloy prefers a c(2 × 2) mixed CuPt underlayer capped with a pure Cu layer as determined by ion scattering studies [27].

## 5. Conclusions

SATLEED and first-principles simulation have been used to determine the structure of Cu{100}–c(2 × 2)–Pt underlayer alloy formed by thermal activation of 0.5 ML Pt adsorbed on Cu{100}. The analysis retrieved a structure that consists of an ordered c(2 × 2) Cu–Pt second layer capped with a pure Cu layer.

The first and second interlayer spacings are found to be expanded by +5.1 ± 1.7 and +3.5 ± 1.7% respectively (relative to the bulk Cu interlayer spacing of 1.807 Å) as a result of insertion of the ∼8% larger Pt atoms into the second layer.

The ordered mixed layer is found to be rippled by 0.08 ± 0.06 Å with Pt atoms rippled outwards towards the solid–vacuum interface.

## Acknowledgements and dedication

EA and AW would like to dedicate this paper to Dr Colin Barnes who died in a tragic fishing accident. Colin was a great enthusiast for science and a good friend. We were in the process

of drafting this paper at the time of Colin's accident. Without his dedication and skill the work presented in this paper would not have been possible. We would also like to thank Mrs Valerie Favry for her help in preparing the figures.

## References

[1] Bardi U 1994 *Rep. Prog. Phys.* **57** 939
[2] Praserthdam P and Majitnapakul T 1994 *Appl. Catal.* A **108** 21
[3] Yoshinbu J and Kawai M 1995 *J. Chem. Phys.* **103** 3220
[4] Graham G W, Schmitz P J and Thiel P A 1990 *Phys. Rev.* B **41** 3353
[5] Belkhou R, Thiele J and Guillot C 1997 *Surf. Sci.* **377** 948
[6] Gorodetski V V, Matveev A V, Cobden P D and Nieuwenhuys B E 2000 *J. Mol. Catal A: Chemical* **158** 155
[7] Hirsimäki M, Suhonen S, Pere J, Valden M and Pessa M 1998 *Surf. Sci.* **402** 187
[8] Nieuwenhuys B E 1996 *Surf. Rev. Lett.* **3** 1869
[9] Hoflund G B, Epling W S and Minahan D M 1999 *Catal. Lett.* **62** 169
[10] Larsen J H and Chorkendorff I 1999 *Surf. Sci. Rep.* **35** 165
[11] Graham G W, Schmitz P J and Thiel P A 1990 *Phys. Rev.* B **41** 3353
[12] Shen Y G, Yao J, O'Connor D J, King B V and MacDonald R J 1996 *Solid State Commun.* **100** 21
[13] Reilly J P, O'Connell D and Barnes C J 1999 *J. Phys.: Condens. Matter* **11** 8417
[14] Barnes C J, AlShamaileh E, Pitkänen T, Kaukasoina P and Lindroos M 2001 *Surf. Sci.* **492** 55
[15] Reilly J P 2001 *PhD Thesis* Dublin City University, Dublin, Ireland
[16] Van Hove M A, Moritz W, Over H, Rous P J, Wander A, Barbieri A, Materer N, Starke U and Somorjai G A 1993 *Surf. Sci. Rep.* **19** 191
[17] Barbieri A and Van Hove M A *Phase Shift Program Package* http://electron lbl gov/leedpack/leedpack html
[18] Kittel C 1986 *Introduction to Solid State Physics* (New York: Wiley) p 110
[19] Pendry J B 1980 *J. Phys. C: Solid State Phys.* **13** 937
[20] Payne M C, Teter M P, Allan D C, Arias T A and Joannapoulos J D 1992 *Rev. Mod. Phys.* **64** 1045
[21] 1999 CASTEP 4 2 Academic Version, licensed under the UKCP-MSI agreement
[22] Vanderbilt D 1994 *Phys. Rev.* B **48** 97
[23] Perdew J P 1986 *Phys. Rev.* B **34** 7406
[24] Fehrenbach G M and Bross H 1993 *Phys. Rev.* B **48** 17703 and references therein
[25] AlShamaileh E and Barnes C J 2002 *Phys. Chem. Chem. Phys.* **4** 5148
[26] Crampin S and Rous P J 1991 *Surf. Sci. Lett.* **224** L137
[27] Shen Y G, O'Connor D J and Wandelt K 1998 *Surf. Sci.* **410** 1